AGU PUBLICATIONS

JGR

Journal of Geophysical Research: Solid Earth

RESEARCH ARTICLE
10.1002/2014JB011337

Key Points:
- Experiments motivated by field observations of heterogeneous fault structure
- Laboratory investigation into the implications of fault zone heterogeneity
- Fault zone structure influences friction constitutive behavior and mode of slip

Correspondence to:
B. M. Carpenter,
brett.carpenter@ingv.it

Citation:
Carpenter, B. M., M. M. Scuderi, C. Collettini, and C. Marone (2014), Frictional heterogeneities on carbonate-bearing normal faults: Insights from the Monte Maggio Fault, Italy, *J. Geophys. Res. Solid Earth*, *119*, doi:10.1002/2014JB011337.

Received 30 MAY 2014
Accepted 28 OCT 2014
Accepted article online 30 OCT 2014

Frictional heterogeneities on carbonate-bearing normal faults: Insights from the Monte Maggio Fault, Italy

B. M. Carpenter[1,2], M. M. Scuderi[2,3], C. Collettini[1,3], and C. Marone[2]

[1]Istituto Nazionale di Geofisica e Vulcanologia, Rome, Italy, [2]Department of Geosciences and Energy Institute Center for Geomechanics, Geofluids, and Geohazards, The Pennsylvania State University, University Park, Pennsylvania, USA, [3]Dipartimento di Science della Terra, Sapienza Università di Roma, Rome, Italy

Abstract Observations of heterogeneous and complex fault slip are often attributed to the complexity of fault structure and/or spatial heterogeneity of fault frictional behavior. Such complex slip patterns have been observed for earthquakes on normal faults throughout central Italy, where many of the M_w 6 to 7 earthquakes in the Apennines nucleate at depths where the lithology is dominated by carbonate rocks. To explore the relationship between fault structure and heterogeneous frictional properties, we studied the exhumed Monte Maggio Fault, located in the northern Apennines. We collected intact specimens of the fault zone, including the principal slip surface and hanging wall cataclasite, and performed experiments at a normal stress of 10 MPa under saturated conditions. Experiments designed to reactivate slip between the cemented principal slip surface and cataclasite show a 3 MPa stress drop as the fault surface fails, then velocity-neutral frictional behavior and significant frictional healing. Overall, our results suggest that (1) earthquakes may readily nucleate in areas of the fault where the slip surface separates massive limestone and are likely to propagate in areas where fault gouge is in contact with the slip surface; (2) postseismic slip is more likely to occur in areas of the fault where gouge is present; and (3) high rates of frictional healing and low creep relaxation observed between solid fault surfaces could lead to significant aftershocks in areas of low stress drop.

1. Introduction

Spatiotemporal variations in the frictional properties of faults are hypothesized to exhibit significant control on earthquake nucleation and earthquake related slip [e.g., *Rice*, 1993; *Boatwright and Cocco*, 1996; *Muhuri et al*., 2003; *Ben-Zion*, 2001; *Parsons*, 2005]. Such variations are hypothesized to result from the dependence of frictional constitutive behavior on-fault conditions such as consolidation state, normal stress, and temperature [e.g., *Marone and Scholz*, 1988; *Blanpied et al*., 1991; *Den Hartog and Spiers*, 2013; *Niemeijer and Vissers*, 2014], the complexity of rheology due to changes in lithology [e.g., *Collettini et al*., 2009; *Ikari et al*., 2013; *Tesei et al*., 2014], and changes in fault structure [e.g., *Ben-Zion and Sammis*, 2003; *Di Stefano et al*., 2011; *Faulkner et al*., 2010; *Collettini et al*., 2011]. Spatial variations in frictional properties and fault strength occur for faults in all tectonic settings [e.g., *Miyazaki et al*., 2004; *Kaneko et al*., 2013; *Noda and Lapusta*, 2013] and are considered to exhibit a first order control on the mode of fault failure.

In central Italy, many of the M_w 6 to 7 earthquakes that occur in the active Apennines rupture steeply dipping normal faults. One such recent event, the 2009 M_w 6.3 L'Aquila earthquake, produced well-documented, complex fault slip [*Di Stefano et al*., 2011; *Chiaraluce*, 2012; *D'Agostino et al*., 2012; *Valoroso et al*., 2013]. Complexity in fault slip has been noted on timescales of earthquake rupture, where slip propagation occurred at different velocities and in various directions, including a momentary pause in rupture [*Di Stefano et al*., 2011], and the postseismic period, where afterslip occurred in distinct patches of the rupture plane [*D'Agostino et al*., 2012; *Cheloni et al*., 2014]. Furthermore, a complex image of the L'Aquila fault has emerged from high-resolution seismology [*Chiaraluce*, 2012; *Valoroso et al*., 2013; *Valoroso et al*., 2014]. Such complexity has been observed for other normal faulting events in central Italy, such as the 1997 Colfiorito sequence [*Chiaraluce et al*., 2003; *Miller et al*., 2004]. This work shows that these earthquakes nucleate at depths of 5–8 km and have aftershocks that extend to shallow depths (<1 km). Furthermore, widespread seismicity is observed throughout central Italy at these depths [*Chiarabba et al*., 2005]. The lithologies at these depths, from the surface to ~10 km, are dominated by thick, carbonate sequences [e.g., *Mirabella et al*., 2008] whose

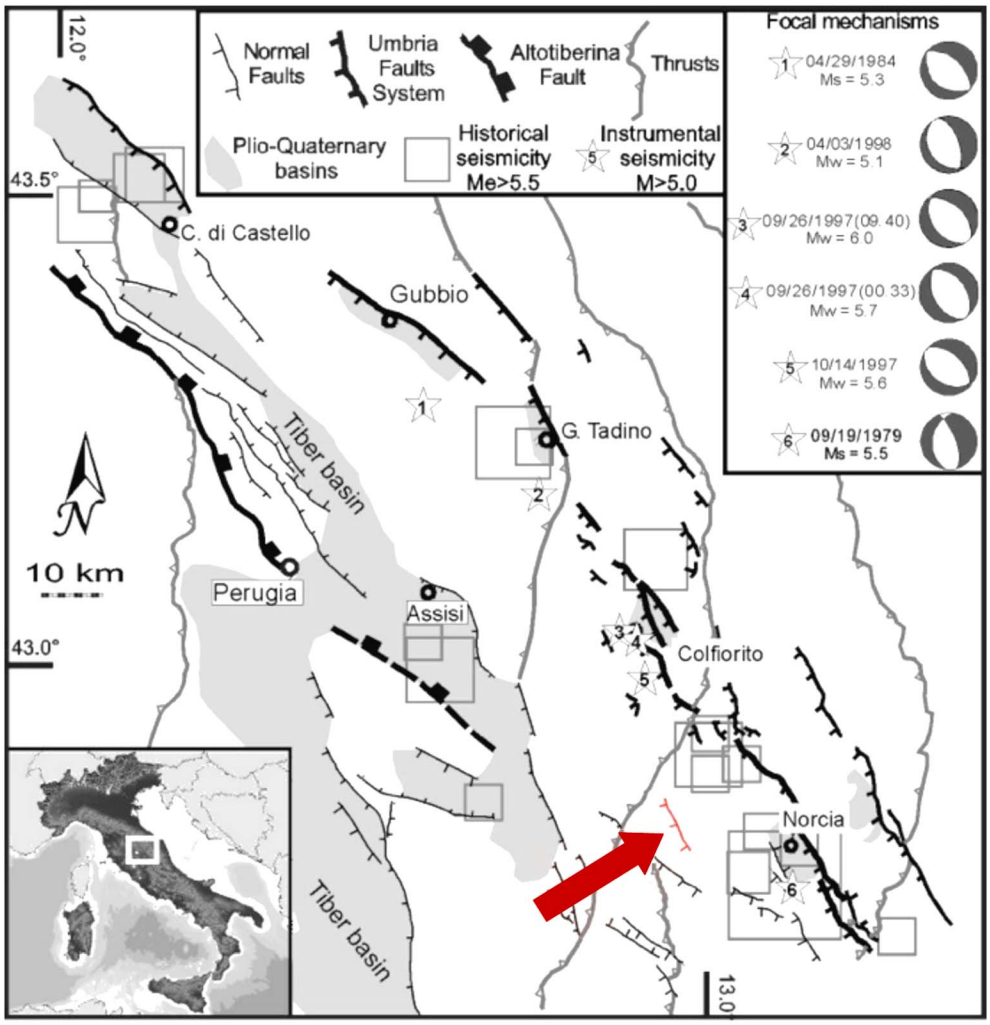

Figure 1. Location and schematic map of the Umbria region in central Italy showing regional fault structures, historical seismicity, and focal mechanisms for the noted events [*Collettini et al.*, 2003, and references therein]. The Monte Maggio Fault (MMF) is identified by the red arrow.

frictional properties under shallow crustal conditions, until recently, have received very little attention [*Collettini et al.*, 2011; *De Paola et al.*, 2011; *Smith et al.*, 2011; *Fondriest et al.*, 2013; *Scuderi et al.*, 2013; *Violay et al.*, 2013].

In order to better understand observations of complex fault slip, we conducted experiments to investigate several sources of complexity using fault rocks representative of those at seismogenic depths. Here we present results from experiments on-fault rocks collected from the Monte Maggio Fault, with the explicit goal of determining how rock type and mechanical complexities in the fault could control variations in earthquake nucleation and fault slip.

2. Geologic Setting and Fault Description

The Monte Maggio Fault (MMF), located in the northern Apennines, is a major structure that aligns with the currently active tectonic setting (Figure 1). Normal faults in the Apennines are known to host some of the largest earthquakes [e.g., *Basili et al.*, 2008; *Chiaraluce*, 2012]. The MMF, exhumed from ~2 km depth, has accommodated approximately 650 m of slip [*Collettini et al.*, 2014] and cuts across lithologies similar to those that hosted the Gubbio 1984, Umbria-Marche 1997, and L'Aquila 2009 earthquake sequences.

This 10 km long structure is particularly well exposed (Figure 2, top) near the town of Rocchetta, Italy. At the kilometer scale, the fault is similar to the structures observed, via high-resolution aftershock mapping of the

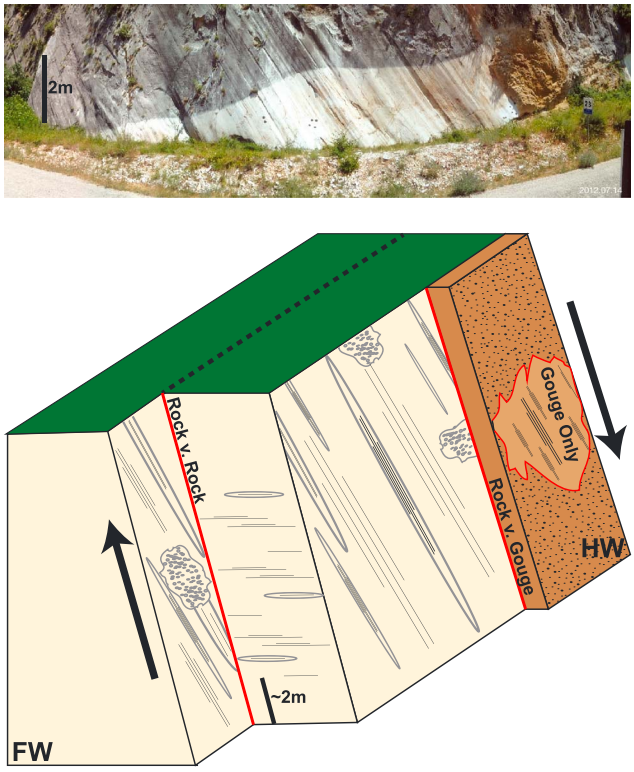

Figure 2. Panoramic outcrop picture of the (top) exposed Monte Maggio fault and (bottom) schematic illustration summarizing our observations of fault structure. We observe three parallel slip surfaces at the outcrop scale (highlighted in red) that all show consistent slip kinematics. The slip surface is highly polished but shows grooves and striations at many scales. Slip is observed in areas where the slip surface brings into contact solid rock versus solid rock, solid rock versus powdered gouge, and powdered gouge only.

fault that produced the 2009 L'Aquila earthquake [*Valoroso et al.*, 2014]. At the outcrop scale, the fault is composed of parallel, distinct slip surfaces extending for a total width of ~50 m (Figure 2), all showing kinematic indicators of fault slip that are consistent with the current, extensional tectonic setting. Fault structure and slip surface phenomena are consistent with observations of other normal faults cutting carbonate lithologies [*Stewart and Hancock*, 1991; *Smith et al.*, 2011; *Bullock et al.*, 2014] and are more fully explored in a separate manuscript [*Collettini et al.*, 2014]. Here we focus on an exceptionally well-exposed fault exposure (Figure 2, top) that separates cataclastic fault rocks derived from the Calcare Massiccio massive limestones (Lower Jurassic) in the footwall and cataclasite, formed mainly from marly limestone of the Bugarone formation (Upper Jurassic-Lower cretaceous) in the hanging wall (Figure 2, bottom). The presence of clay in the hanging wall fault rock enhances pressure solution processes [e.g., *Gratier et al.*, 2013; *Viti et al.*, 2014] as indicated by the development of an intense network of stylolites and mineral precipitation as indicated by an extensive calcite fracture system that is perpendicular to the stylolites [*Collettini et al.*, 2014]. At the exposed outcrop, undeformed hanging wall material is not present.

Excellent exposure of the fault allowed us to identify slip surfaces separating different types of fault rocks. We observe distinct slip surfaces within massive limestone (i.e., solid rock versus solid rock), massive limestone versus gouge (i.e., solid rock versus gouge), and solely within gouge (Figure 2, bottom). In cases where gouge is present, it is derived from both the massive limestone of the footwall and marly limestone of the hanging wall. The complexity of this fault structure, with multiple closely spaced slip surfaces and different mechanical contacts, would likely lead to complex slip patterns during earthquake rupture and post seismic slip. Furthermore, differences in the frictional behavior of the different slip patches would also likely control processes involved in earthquake nucleation and the restrengthening of the fault after dynamic failure.

3. Experimental Methods

3.1. Experimental Samples

In order to evaluate the complexity observed at the outcrop scale, we collected three sets of samples. Our samples are representative of the full range of fault rocks and include (1) solid rock versus solid rock, (2) solid rock versus powdered gouge, and (3) powdered gouge. We collected many samples, both intact pieces and gouge/rubble, to ensure a representative sampling of both the hanging wall cataclasite and footwall limestone. In order to collect intact specimens of the fault surface, we cored the fault surface in areas of relatively uniform surface topography and without noticeable fractures (Figures 3a and 3b). In a few areas, the hanging wall cataclasite was both competent and thin enough to core across a principal slip zone (PSZ, Figure 3c). In these

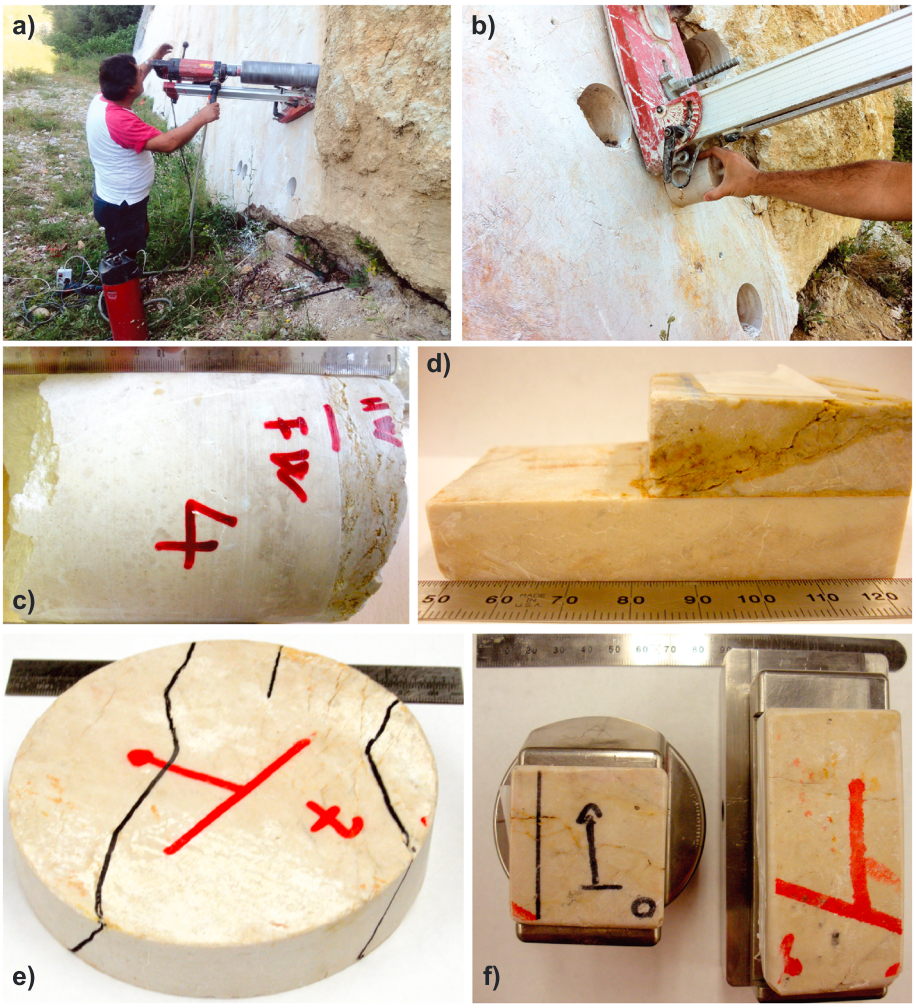

Figure 3. (a, b) Sampling of the fault surface and fault contact was accomplished via coring that produced 12 cm diameter core. (c) Recovered and (d) prepared experimental sample containing the hanging wall-footwall contact. (e) Recovered and (f) prepared experimental sample of the polished slip surface. Structural features highlighted in black (Figure 3e) are antithetic, small displacement faults that are healed/sealed and merged into the slip surface.

few areas, it is clear that the healed PSZ survived exhumation and subsequent sampling. Scanning electron microscope observations taken across the PSZ show evidence for multiple slip events along this single surface including evidence of calcite decarbonation that would result from seismic slip [*Collettini et al.*, 2014].

Samples of the intact PSZ and fault surface were carefully cut into L-shaped blocks for experiments (Figure 3d), making sure not to reactivate the healed PSZ or small displacement, antithetic faults found in both the hanging wall and footwall (Figures 3d–3f). Subsequently, the nonsliding faces of these blocks were surface ground flat and parallel to ensure even stress distribution and prevent fracturing. Our sample collection and preparation provided three sample types: (1) intact PSZ (Figure 3d), (2) intact fault rock including the fault surface (Figures 3e and 3f), and (3) samples of the footwall and hanging wall that were pulverized and sieved to a grain size $<150\,\mu m$. The footwall and slip surface samples are mainly composed of calcite (>98%), whereas the hanging wall marly cataclasite is mostly calcite but contains a minor amount (~10%) of smectite [*Viti et al.*, 2014].

3.2. Experimental Procedures and Sample Configurations

We performed experiments in six different configurations (Figure 4a and Table 1). These included the following: (1) refractured and sheared samples of an intact fault surface (SS/Cc), (2) samples of the shear surface that were collected from separate locations and sheared as solid blocks (SS/SS), (3) powdered gouge composed of the slip surface sheared against the intact slip surface (SS/pSS), (4) powdered gouge of

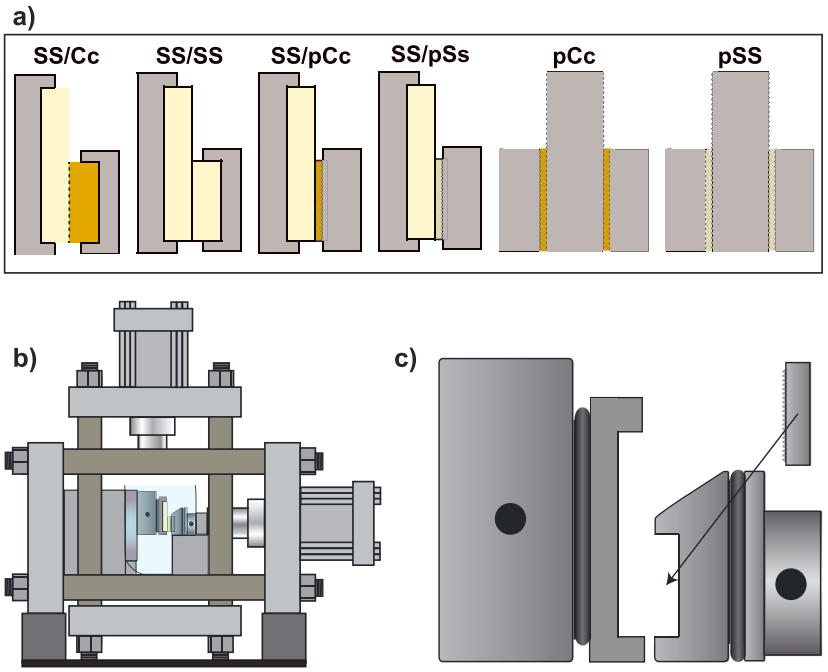

Figure 4. (a) The six configurations of shear used in this study. See text for full descriptions. The hanging wall cataclasite is shown in gold, whereas the footwall limestone is shown in yellow. (b) Pennsylvania State University Rock and Sediment Mechanics Laboratory biaxial deformation apparatus used in this study. The schematic shown is for the single-direct shear setup. Water was contained in a plastic membrane during the experiment to maintain sample saturation. (c) Zoom of the single direct forcing blocks as used for shearing intact samples of the fault. The grooved platen is used when shearing gouge against an intact part of the fault surface. The double-direct configuration is not shown [see *Ikari et al.*, 2007].

the hanging wall cataclasite sheared against the intact slip surface (SS/pCc), (5) powdered gouge of the principal slip surface (pSS), and (6) powdered gouge of the hanging wall cataclasite (pCc). Configurations 1–4 were done in single-direct shear (Figure 4c) and configurations 5 and 6 were done in the double-direct shear configuration.

We performed our experiments under saturated conditions at room temperature. Intact samples were vacuum saturated for a minimum of 12 h, but typically longer, before each experiment. Deionized water was combined with limestone rubble and gouge and allowed to equilibrate at room temperature for ~4 days. This allowed the solution to be in equilibrium with $CaCO_3$ at room temperature prior to experiments. Previous work indicates that the chemical equilibrium conditions for a $CaCO_3$–H_20–CO_2 system is reached within 48 h under conditions near room temperature [*Sjoberg and Rickard*, 1984] and has shown that pore fluid chemistry has a significant impact on the rates of calcite solution/precipitation [*Zhang and Spiers*, 2005]. By using a solution at equilibrium with $CaCO_3$ under our experimental conditions, we ensured that changes in pore fluid chemistry did not play a role in the mechanical behavior during our experiments. Additionally, we feel a solution at equilibrium with $CaCO_3$ is a better representation of the pore fluid at depth.

Table 1. Experiments and Conditions

Experiment No.	Configuration	Normal Stress (MPa)	Velocity Steps (μm/s)	Slide-Hold-Slides (s)
p3675	SS/SS	10	1–300	3–1,000
p3676	SS/pSS	10	1–300	3–1,000
p3678	pSS	10	1–300	3–1,000
p3769	SS/Cc	10	1–300	3–1,000
p3770	SS/pCc	10	1–300	3–1,000
p3772	pCc	10	1–300	3–1,000
p3773	SS/Cc	10	1–300	3–1,000
p3938	SS/SS	10	X	1–10,000

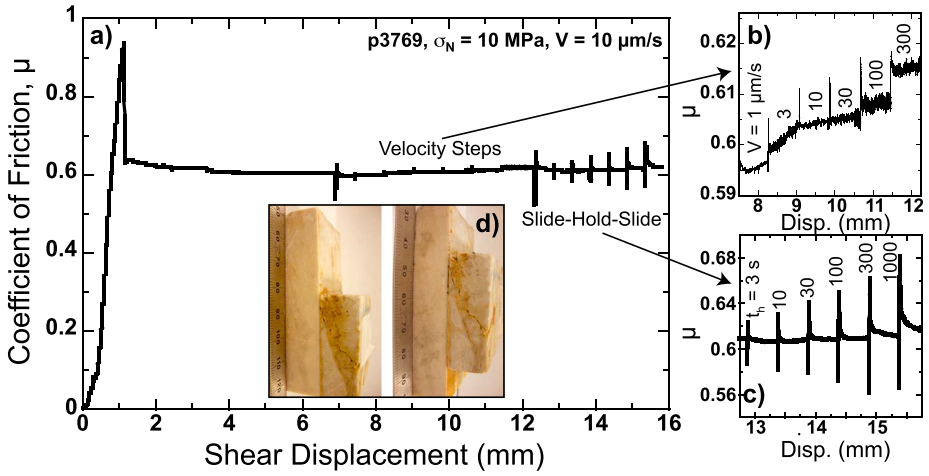

Figure 5. (a) Representative friction versus shear displacement curve for the SS/Cc sample configuration. Refer to Figure 4a and the text for a description of each configuration. Details of the (b) velocity-stepping and (c) slide-hold-slide procedures used to evaluate the friction constitutive properties. (d) The observed stress drop of 3.3 MPa in Figure 5a results from the reactivation of the fault surface as shown in before and after pictures of the experimental sample.

Experimental samples were removed from the solution, prepared quickly, and placed into the biaxial load frame (Figure 4b). A normal stress of 1 MPa was applied and the $CaCO_3$ solution was added to a flexible, plastic membrane surrounding the sample. As experiments with gouge were prepared dry, all samples were allowed to saturate for 1 h at low normal stress (~1 MPa). Subsequent to saturation, normal stress was increased to 10 MPa, and the sample, through monitoring sample compaction, was allowed to reach a quasi steady state of mechanical compaction. Stresses were measured to ± 2kPa using strain-gauge load cells and displacements were measured continuously to ± 0.1 μm using direct current displacement transducers throughout the experiment. All experimental data were recorded at 10 kHz and then down sampled to 1–1000 Hz based on the shearing velocity. Next, samples were sheared for 5–7 mm at 10 μm/s as a shear "run-in" phase (Figure 5a), meant to produce a relatively uniform surface roughness for rock-on-rock experiments, to develop a steady state fabric [e.g., *Haines et al.*, 2013] within the gouge layers, and to reach a mechanical steady state. Peak and steady state friction values are measured during this portion of the experiment (Figure 6). Once steady state friction was obtained, velocity-stepping and slide-hold-slide tests were performed to measure frictional velocity dependence and frictional healing, respectively (Figures 5b and 5c). In velocity-stepping tests, the load point velocity is increased stepwise from 1, 3, 10, 30, 100, and 300 μm/s, with 0.5 mm of shear at each step. During slide-hold-slide (SHS) tests, the load point is held stationary for hold times of 3, 10, 30, 100, 300, and 1000 s, with 0.5 mm of shear at 10 μm/s after each hold. One additional experiment, with holds up to 10,000 s was performed to determine frictional healing at longer timescales and provide a check of reproducibility for one of the more complex sample arrangements.

Velocity-stepping tests are used to determine the velocity dependence of friction via the friction rate parameter (*a-b*):

$$(a\text{-}b) = \Delta\mu_{ss}/\Delta \ln V \tag{1}$$

where μ_{ss} is the steady state friction coefficient and V is sliding velocity [e.g., *Marone*, 1998]. Positive values of (*a-b*), termed velocity strengthening (Figure 7a), are associated with stable sliding and inhibit rupture nucleation. Negative values, termed velocity weakening (Figure 7a), are a prerequisite for unstable slip and earthquake nucleation. We determined values of *a-b* and other constitutive parameters by fitting our data using an inverse modeling technique [e.g., *Blanpied et al.*, 1998] with *Dieterich*'s [1979] time-dependent friction law with two state variables:

$$\mu = \mu_0 + a \ln (V/V_0) + b_1 \ln (V_0\theta_1/D_{c1}) + b_2 \ln (V_0\theta_2/D_{c2}) \tag{2}$$

$$\mathrm{d}\theta_i/\mathrm{d}t = 1 - (V\theta_i/D_{ci}), \ (i = 1, 2) \tag{3}$$

where a, b_1, and b_2 are empirically derived constants (dimensionless), θ_1 and θ_2 are state variables with units of time, and D_{c1} and D_{c2} are critical slip distances [e.g., *Marone*, 1998]. We used a time-dependent state

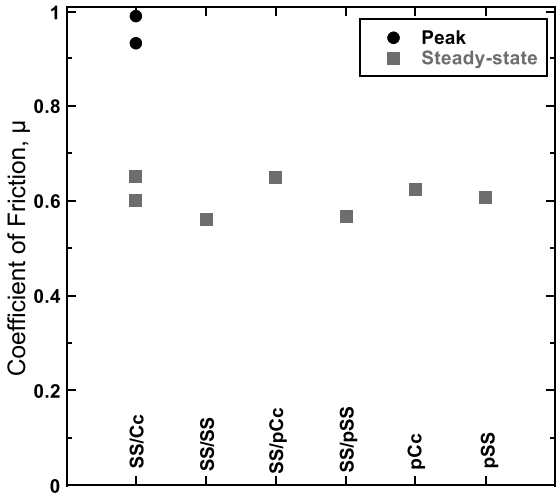

Figure 6. Peak and steady state coefficient of friction values for each configuration studied. Peak values were only observed in the SS/Cc configuration where the fault contact was rebroken. Refer to Figure 4a and the text for a description of each configuration.

evolution law [*Dieterich*, 1979; *Ruina*, 1983], although we recognize that friction state evolution may be better described by a slip-dependent law in some cases [*Bayart et al*., 2006; *Marone and Saffer*, 2014]. Most of our data are fit well by a one state variable friction law ($b_2 = \theta_2 = 0$), making the last term of equation (2) unnecessary. However, some of our data required two state variables. We report values of (a-b), a, b, and D_c and define $b = b_1 + b_2$ and $D_c = D_{c1} + D_{c2}$ to compare one and two state variable cases. Typical standard deviation error bars from modeling are smaller than the symbol size.

Slide-hold-slide tests are used to assess rate/state friction behavior under slow velocity and to determine the amounts of frictional healing and creep relaxation. These tests provide an approximate analog for the seismic cycle, where the fault slips, experiences an interseismic period, and then slips again. By varying the hold time, we determine the rates of frictional healing (β) and creep relaxation (β_c):

$$\beta = \Delta\mu / \log_{10} t_h, \tag{5}$$

$$\beta_c = \Delta\mu_c / \log_{10} t_h, \tag{6}$$

where $\Delta\mu$ is the increase in peak friction after a hold of time t_h, relative to the initial value of sliding friction and $\Delta\mu_c$ is the decrease in friction during the hold, relative to the initial value (Figure 8a). The parameter β provides an estimate of the rate of fault healing and the rate of change of seismic stress drop with earthquake recurrence time. Positive healing rates, along with velocity-weakening friction behavior, are likely required for repeated earthquakes on the same fault or fault patch [*Brace and Byerlee*, 1966; *Dieterich*, 1978]. Furthermore, the creep relaxation that occurs during a hold can be related to earthquake afterslip [*Marone et al*., 1991] and rate/state friction properties [*Beeler et al*., 1994; *Marone*, 1998].

4. Results

4.1. Frictional Strength

We find a near constant value of steady state friction (μ = ~0.6), regardless of the sample configuration (Figure 6). For the experiments that refractured the slip surface (Figure 5), we observe values of peak friction of μ = ~0.95 that directly precede a shear stress drop, equivalent to ~3.3 MPa. Our values for frictional strength are consistent with other reported values for limestone and calcite-rich fault rocks at low stress and room temperature [*Weeks and Tullis*, 1985; *Carpenter et al*., 2011; *Scuderi et al*., 2013; *Verberne et al*., 2010; *Verberne et al*., 2013; *Tesei et al*., 2014].

4.2. Velocity Dependence of Friction

We observe complex rate-dependent behavior that depends on both the sample configuration and velocity (Figure 7). Experiments where the frictional interface is rock on rock (SS/Cc and SS/SS) show strong velocity-strengthening behavior at our lowest velocity, a transition to velocity-weakening behavior at intermediate velocities (V = 10 and 30 μm/s), and then become increasingly velocity strengthening at higher slip velocity. Experiments on samples involving powdered slip surface and cataclasite (SS/pSS, SS/pCc, pSS, and pCc) show velocity-weakening to velocity-neutral frictional behavior at low velocities and a transition to velocity-strengthening frictional behavior at our highest velocity tested (Figure 7). The largest negative values of (a-b) are observed in experiments where two slip surfaces are sheared against one another. The velocity dependence results for experiments involving powdered samples are broadly consistent with previous work on calcite-rich samples under similar experimental conditions [*Scuderi et al*., 2013; *Verberne et al*., 2010, 2013; *Tesei et al*., 2014].

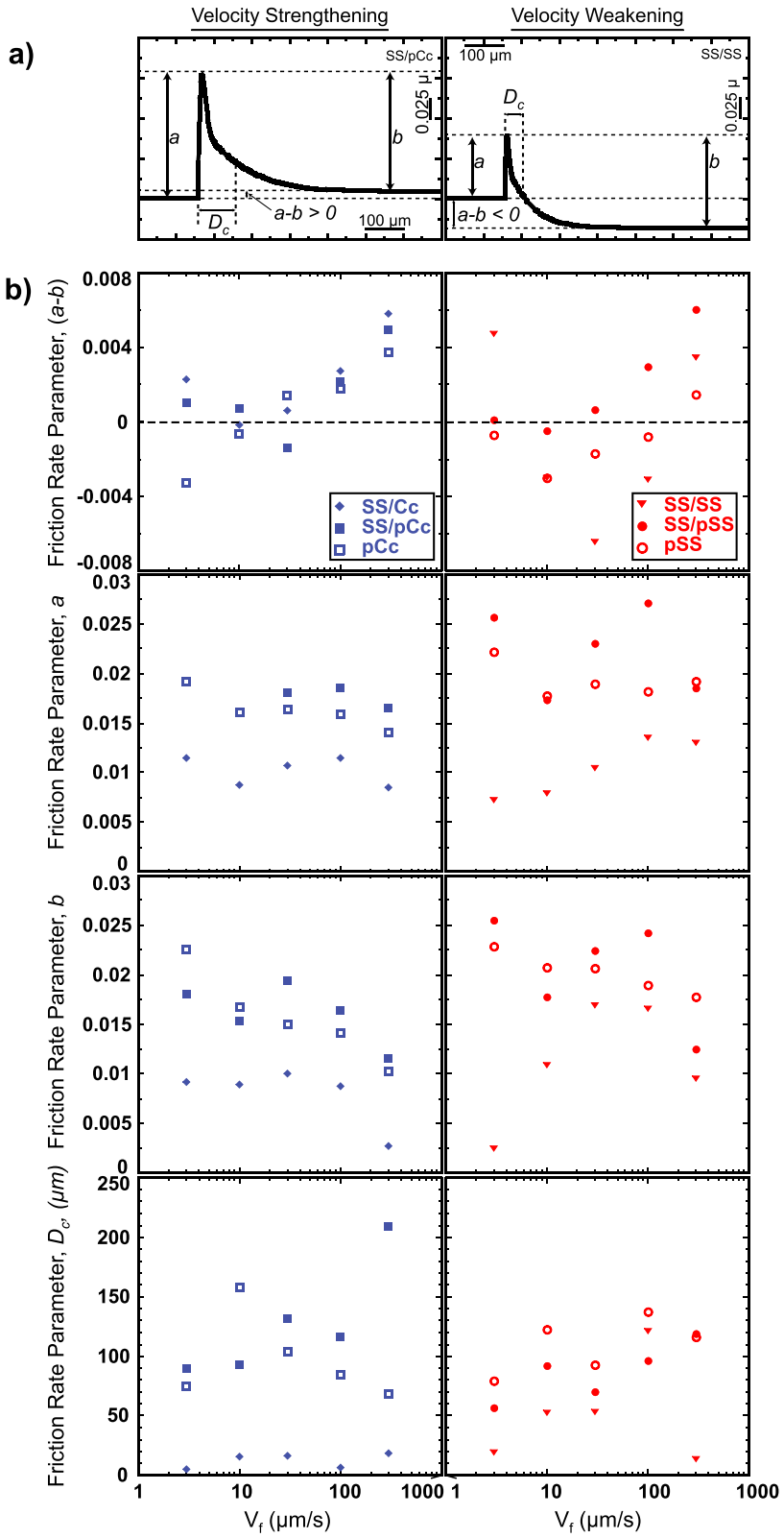

Figure 7. (a) Schematic illustrations showing the frictional constitutive parameters *a*, *b*, D_c and *a-b* for velocity-strengthening and velocity-weakening cases. (b) The evolution of frictional rate parameters, *a-b*, *a*, *b*, and D_c, with velocity. Sample configurations involving the hanging wall cataclasite are shown on the left, whereas sample configurations involving the slip surface are shown on the right. Refer to Figure 4a and the text for a description of each configuration.

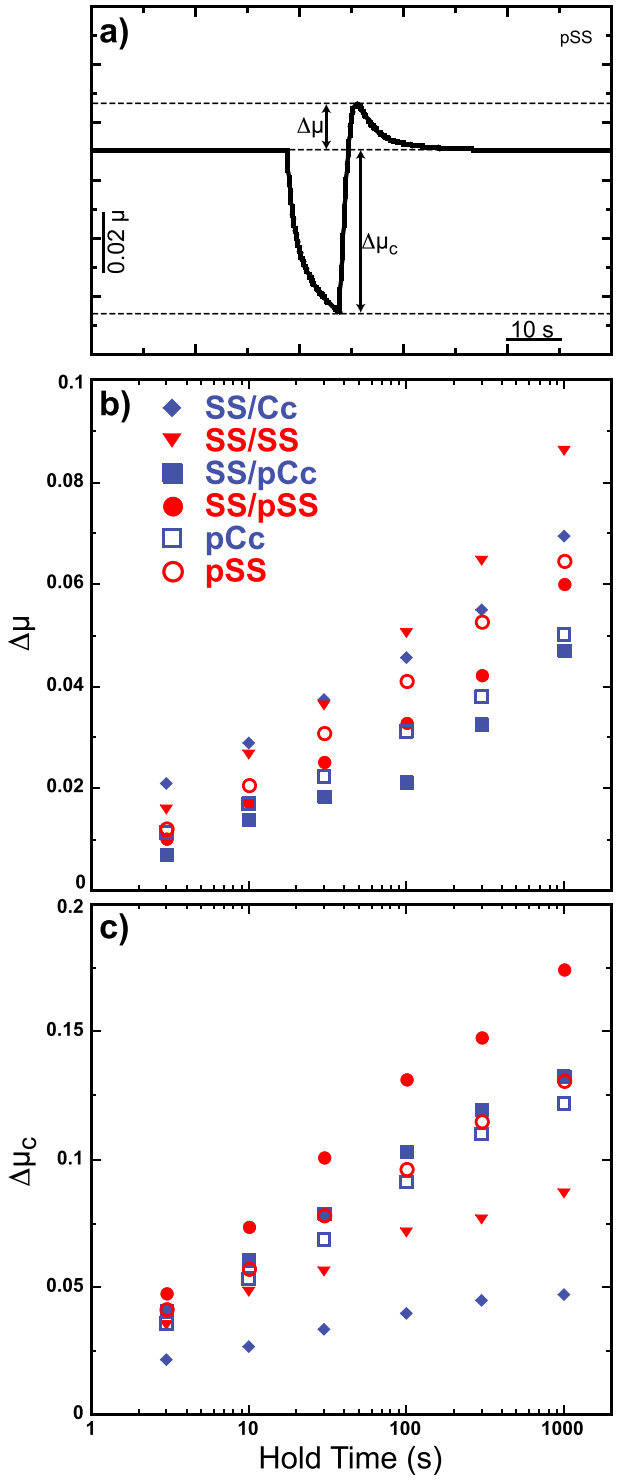

Figure 8. (a) Schematic illustration showing how frictional healing ($\Delta\mu$) and creep relaxation ($\Delta\mu_c$) are measured. (b) Frictional healing versus hold time for each experimental configuration. (c) Creep relaxation versus hold time for each experimental configuration. Refer to Figure 4a and the text for a description of each configuration.

Our results for the friction rate parameters, *a*, *b*, and D_c, show consistent differences between experiments with solid surfaces and experiments with powdered gouge (Figure 7). We observe lower, and relatively constant values of the friction rate parameter, *a*, termed the direct effect, with increasing velocity in experiments involving only solid rocks. Data for experiments involving powdered gouge consistently show higher values of *a*, and no dependence on velocity.

We generally observe lower values of the friction rate parameter, *b*, termed the evolution effect, in experiments involving only solid rocks. We observe no discernable relationship between *b* and shearing velocity in these experiments. However, in experiments on samples of only powdered gouge, we observe a decrease of the friction rate parameter, *b*, with increasing velocity (Figure 7).

Our lowest values ($\leq$10 μm) of D_c, the critical slip distance, are observed in experiments between solid pieces of the principal slip surface and hanging wall cataclasite (SS/Cc). We also observe low values of the critical slip distance in experiments between solid pieces of the principal slip surface (SS/SS). Our data show a weak relationship between D_c and shearing velocity for experiments where powdered gouge is sheared against solid rock (SS/pCc and SS/pSS), as D_c increases with increasing velocity. Values of D_c for experiments involving only powdered gouge are approximately 100 μm and show no consistent relationship with velocity (Figure 7). Our measurements for D_c are consistent with previous work on other rock types that shows smaller values of D_c for solid surfaces when compared to gouge [e.g., *Marone*, 1998, and references therein].

4.3. Frictional Healing and Creep Relaxation

Data from experiments performed between solid rocks show our largest values of healing with experiments between solid pieces of the slip surface (SS/SS) exhibiting a frictional healing value ($\Delta\mu$) of ~0.09 at a hold time of 3000 s (Figure 8b). We also find that sample configurations involving the hanging wall cataclasite consistently show lower values of healing than their slip surface equivalents, likely

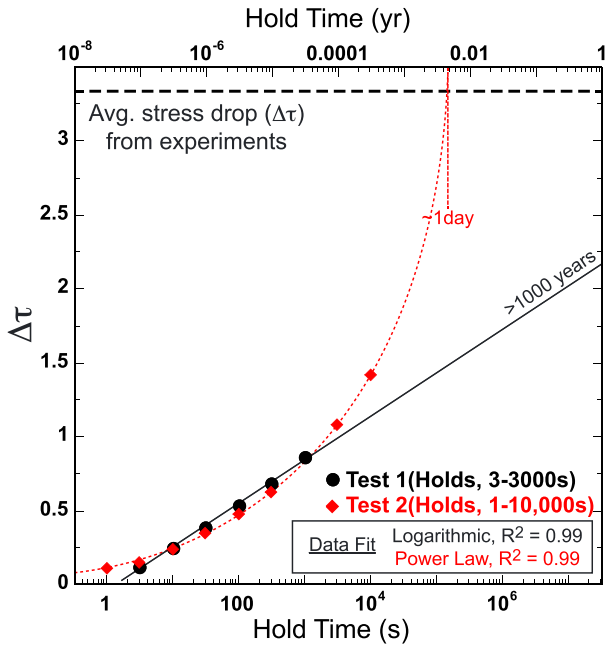

Figure 9. The amount of frictional healing (cast in terms of shear stress) versus hold time for two experiments using the same experimental configuration (SS/SS), and under the same conditions. Horizontal dashed line shows the average stress drop for the two experiments that refractured the fault surface. We show a typical logarithmic fit for Test 1 data (solid, black line) and a power law fit for Test 2 data (red, dashed line). Refer to Figure 4a and the text for a description of each configuration.

due to the presence of phyllosilicates found within the hanging wall cataclasite [*Bos and Spiers*, 2000]. Our values for frictional healing are consistent with other experiments performed on calcite-rich fault gouge under similar conditions [*Carpenter et al*., 2011; *Tesei et al*., 2014]

Our results from creep relaxation show that sample configurations SS/SS and SS/Cc exhibit the lowest values of creep relaxation (Figure 8c) with the SS/Cc configuration showing by far the least amount of any configuration. Our results also show that sample configurations involving the principal slip surface consistently show more creep relaxation than their cataclasite equivalents. We observe our highest values of creep relaxation in experiments performed between the solid slip surface and powdered gouge of that slip surface (SS/pSS).

5. Discussion

5.1. Evolution of Fault Strength

The evolution of fault strength during the seismic cycle determines key earthquake source parameters including stress drop and recurrence interval [e.g., *Scholz*, 2002]. Recent experimental observations of frictional healing indicate that faults can experience little to no frictional healing, or relatively high healing depending on the mineralogical composition of gouge present within the fault [*Carpenter et al*., 2011]. Furthermore, it is generally assumed that time dependence of frictional healing occurs in log-linear fashion and is supported by observations of increasing stress drop with recurrence interval for repeating earthquakes along the Calaveras Fault [*Marone et al*., 1995; *Peng et al*., 2005]. However, several experimental studies suggest that healing data can also be fit equally well with a power law function [*Karner et al*., 1997; *Olsen et al*., 1998; *Nakatani and Scholz*, 2004; *Yasuhara et al*., 2005; *Renard et al*., 2012; *Collettini et al*., 2013]. The rate at which faults restrengthen and regain the ability to sustain subsequent earthquakes, remains an open question. Furthermore, whether this rate is best represented as a logarithmic function or a power law function has significant implications for seismic hazards and could provide insights into the processes governing frictional strength recovery.

In light of these recent observations, we performed an additional SHS experiment in the SS/SS configuration with holds ranging from 1 to 10,000 s. Additionally, this test allows us to show the good repeatability of our data in our most difficult experimental configuration. We note that we were not able to hold our sample as long as previous work, 180,000 s [*Renard et al*., 2012] and 300,000 s [*Nakatani and Scholz*, 2004]. We show that for our complete series of holds in the additional experiment, from 1 to 10,000 s, our data (Figure 9) are better captured by a power law function, whereas in our initial experiment, with holds of 3 to 1000 s, the data are better fit with a logarithmic function. Previous work concerning this issue has tended to favor a logarithmic fit to the data [*Bos and Spiers*, 2002; *Nakatani and Scholz*, 2004; *Renard et al*., 2012]. We also highlight that between 3 and 1000 s, our data from both tests show excellent agreement. In terms of strength recovery on the frictional interface, the difference between the two functions and its implications for subsequent earthquake stress drop are quite evident. The power law fit indicates that it is possible to recover a 3 MPa stress drop in ~1 day, whereas the logarithmic fit indicates a time period of greater than 1000 years (Figure 9). While these differences are obviously significant and important, we note that our data represent only a single sample under one set

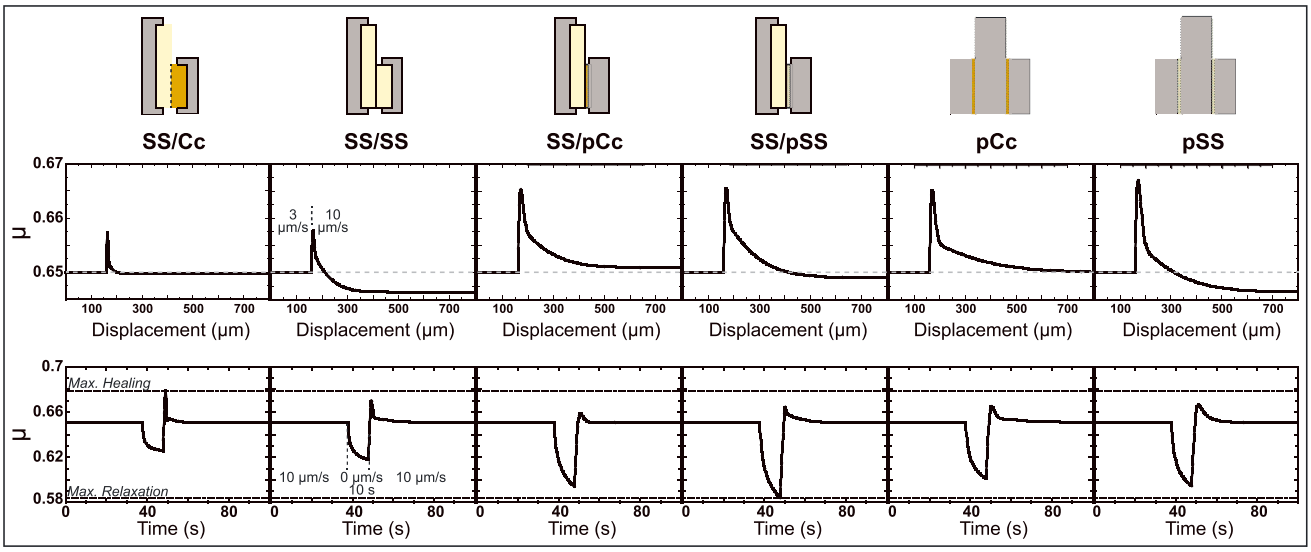

Figure 10. (top) Schematic of each sample configuration. (middle) Modeled friction versus displacement curves for the 3 μm/s to 10 μm/s velocity step for each configuration. Note the dramatically different friction behaviors for the range of samples. Dashed line shows velocity-neutral frictional behavior. (bottom) Modeled friction versus time curves for the 10 s hold for each sample configuration. Note the dramatically different healing and creep relaxation behavior based on sample configuration. Dashed lines show maximum measured healing and creep relaxation amounts for this specific hold. For Figure 10 (middle and bottom), μ_0 was set equal to 0.65.

of conditions, and that, additional experiments with longer hold times are needed. We note also that our experiments were run under conditions of low stress and room temperature but that one might expect an increase in healing, and likely lithification, at increased depths as solution transfer processes become more effective [e.g., *Karner et al.*, 1997; *Blanpied et al.*, 1998; *Muhuri et al.*, 2003; *Tenthorey et al.*, 2003; *Nakatani and Scholz*, 2004; *Yasuhara et al.*, 2005; *Faulkner et al.*, 2010]. Frictional healing in our experiments arises from several factors: (1) a reduction in porosity [*Niemeijer et al.*, 2008] and growth of contact area [e.g., *Dieterich and Kilgore*, 1994] due to the mechanical compaction of our sample; (2) a further decrease in porosity due to pressure solution [e.g., *Niemeijer et al.*, 2008], along with an increase in size and quality of the contact area due to solution transfer processes that would be active under our experimental conditions [e.g., *Renard et al.*, 2012]. The rate of pressure solution is expected to increase with depth, up to 5–7 km [*Gratier et al.*, 2013] and thus would exert influence over the behavior of calcite in the seismogenic zone of the northern Apennines (1–10 km). As a combination of frictional and solution transfer processes are occurring in our samples, we would expect this behavior to be amplified at depths from 2 to 5 km. This interpretation is supported by previous experimental work on calcite-rich rocks, which shows a transition to frictionally unstable behavior at temperatures above 80°C [*Verberne et al.*, 2013] and observations of fault zone lithification observed at the MMF outcrop. We do recognize, however, that there is a complex interplay between stress, temperature, and time that controls the rate of pressure solution [e.g., *Gratier et al.*, 2013].

5.2. Constitutive Properties and Heterogeneous Slip

Friction constitutive behavior varies significantly as a function of rock type and mechanical fault contact (Figures 7 and 8). Comparison of the raw friction data for various configurations can provide insight on-fault slip heterogeneity and the evolution of friction (stress) during earthquake nucleation and propagation. We focus in particular on velocity step tests and details of the friction response during slide-hold-slides. Figure 10 shows modeling results for a velocity step from 3 μm/s to 10 μm/s and a slide-hold-slide sequence with a hold of 10 s.

Comparing the velocity-stepping curves in Figure 10, the small direct effect (friction rate parameter a) and rapid evolution (small values of D_c) to equal or lower values of frictional strength are evident for the SS/Cc and SS/SS configurations. This indicates that fault segments with rock-on-rock sliding will have less resistance to slip acceleration and a much shorter evolution to a new frictional strength, inasmuch as values of D_c are generally lowest in the 3–100 μm/s velocity range (Figure 7). This behavior would promote earthquake

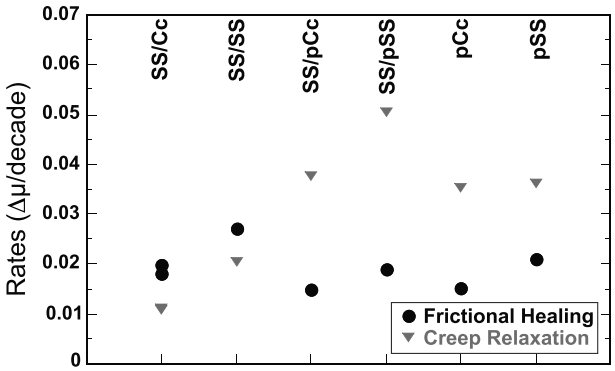

Figure 11. The rates of frictional healing and creep relaxation for each experimental configuration. Note that all samples involving powdered gouge exhibit higher creep relaxation rates than healing rates, whereas sample configurations involving intact samples, show the opposite. Refer to Figure 4a and the text for a description of each configuration.

nucleation and propagation in such areas of a fault. On the other hand, in areas where the frictional interface includes fault gouge, we observe a much larger direct effect, and larger critical slip distances, D_c. Larger values of a and D_c, combined with the fact that these configurations exhibit velocity-neutral frictional behavior, could lead to a slowing of the rupture as it encounters these areas, albeit while allowing continued propagation. The critical slip distance is an important factor that governs some fundamental aspects of earthquake rupture and fault slip. As it is the distance over which friction breaks down (contacts evolve), variations in D_c, when combined with the friction rate parameter (a-b) can be used to determine the propensity for rupture nucleation and propagation [e.g., *Marone and Kilgore*, 1993; *Marone*, 1998].

The slide-hold-slide curves also provide information in terms of postseismic slip and the ability of a slipped fault patch to host subsequent dynamic failure in the form of aftershocks. The amount of creep relaxation in slide-hold-slide tests is proportional to earthquake afterslip, as in both cases, the stored elastic energy surrounding the gouge zone is released through creep and stress relaxation [*Marone and Saffer*, 2014]. Additionally, the amount of frictional healing is indicative of how quickly the fault recovers the frictional strength it lost during earthquake rupture. These curves show that faults defined by solid surfaces will heal much more quickly and experience far less post seismic slip than areas where significant fault gouge is present (Figure 10). Furthermore, our results show that areas of the fault that have slipped and where gouge is present are likely to experience significant postseismic slip, as this is favored by their velocity-neutral frictional behavior, large critical slip distances, and considerable creep relaxation. Our results also suggest that areas where the fault is defined by a rock-on-rock contact and experience minor on-fault seismic slip, would be prone to host aftershocks quickly after the main shock due to their low values of creep relaxation, rapid healing, and velocity-weakening friction behavior. Our results are consistent with experiments that show enhanced pressure solution creep in samples that have been dynamically shocked and suggest that as the sample heals, pressure solution creep is reduced [*Gratier et al*., 2014]. Our results show that samples that exhibit the highest healing rates also exhibit the lowest amounts of creep relaxation and vice versa (Figure 11).

It has recently been suggested that the competition between strengthening (healing) and stress relaxation (creep relaxation) mechanisms exhibits an important control on a fault's mode of slip [*Carpenter et al*., 2011; *Marone and Saffer*, 2014]. An important consideration in the transition from stable, aseismic sliding, to repeated earthquake failure is that the rate of fault restrengthening must be large enough to overcome the rate of stress relaxation that results from plastic deformation and creep [*Marone and Saffer*, 2014].

Previous work has observed that samples that exhibit frictional healing rates equal to or greater than the creep relaxation rate are derived from faults that tend to fail in earthquakes rather than via aseismic slip [*Carpenter et al*., 2011]. Our results for healing and creep relaxation rates (Figure 11) support this hypothesis and our interpretations of faults with rock on rock contacts favoring rupture nucleation. Additionally, our data show that areas of the fault where the creep relaxation rate is larger than the frictional healing rate would support rupture propagation and other mixed modes of fault slip.

Our data documenting how fault heterogeneities influence the mechanical behavior of carbonate-bearing faults may provide some insight into observations of complex fault slip for the 2009 L'Aquila earthquake. We recognize that as our experiments were performed at low stress and room temperature, the extrapolation to depth should be done carefully. However, the observations that (1) the rate of pressure solution should increases with depth, to 5 km, and then remains relatively constant to greater depths, and (2) the experiments on calcite-rich gouge performed at elevated temperature show the gouge transitions from velocity-

strengthening to velocity-weakening frictional behavior at a temperature of 80°C, likely due to enhanced solution transfer processes [*Verberne et al*., 2013], indicate that the mechanical data we observe would be enhanced at greater depths, allowing us to extrapolate our data.

Di Stefano et al. [2011] showed that the main shock of the 2009 L'Aquila earthquake nucleated in an area of high *P* wave velocity (V_p) and low Poisson's ratio, possibly indicating a zone of more competent rock and solid fault contact compared to the surrounding areas. This is supported by laboratory data on samples recovered from the MMF that show that the hanging wall cataclasite has a lower V_p and higher Poisson's ratio than the more competent, footwall limestone [*Trippetta et al*., 2013]. Furthermore, combining the results of *D'Agostino et al*. [2012] and *Di Stefano et al*. [2011] shows that two of the three areas of intense afterslip are located in areas of low V_p and high Poisson's ratio, consistent with the possible occurrence of gouge with velocity-neutral frictional behavior, large critical slip distances, and considerable creep relaxation. A further contribution to afterslip might be induced by pressure solution creep along phyllosilicate-rich portions of the fault zone [e.g., *Gratier et al*., 2013], like those formed from marly protolith along the Monte Maggio structure. Finally, the delayed area of rupture identified by *Di Stefano et al*. [2011] and *Cirella et al*. [2012] is also an area of increased rise time [*Cirella et al*., 2012], which is consistent with our frictional data for a gouge-rich fault showing a larger resistance to increased velocity slip than areas where the fault cuts solid rock.

6. Summary

We present results from experiments designed to test how differences in fault rock and fault contact, as observed naturally in the field, affect the mechanical behavior of an exposed, carbonate-bearing normal fault. We use several shear configurations to reproduce the complexity observed in natural fault zones. Our results indicate that (1) earthquake nucleation is favored on areas of the fault where the slip surface separates massive limestone, with propagation likely into areas where fault gouge is in contact with the slip surface; (2) postseismic slip is more likely to occur in areas of the fault where gouge separates the hanging wall and footwall; and (3) the high healing and low creep relaxation rates observed between solid fault surfaces would allow for significant aftershocks in areas of low stress drop. Furthermore, our data may partially explain the complex slip behavior observed during and after the 2009 L'Aquila earthquake if the observed behavior is due to rheological differences in the fault contact. Our work has documented fault heterogeneities in the field and showed how these heterogeneities could lead to heterogeneous frictional properties, which in turn may result in complex fault slip.

Acknowledgments

This research was carried out within the ERC Starting Grant GLASS (259256) to C.C. B.M.C. was partially funded by the National Science Foundation, under grants EAR054570, EAR0746192, and OCE-0648331 to C.M., during early portions of this study. We thank J. Gratier and M. Pec for thoughtful and detailed reviews, which significantly improved this manuscript. We also thank Steve Swavely for technical assistance in the laboratory and Luisa Valoroso and Telemaco Tesei for useful discussions during the development of this manuscript. Our data are available by FTP transfer by contacting the corresponding author.

References

Basili, R., G. Valensise, P. Vannoli, P. Burrato, U. Fracassi, S. Mariano, M. M. Tiberti, and E. Boschi (2008), The Database of Individual Seismogenic Sources (DISS), version 3: Summarizing 20 years of research on Italy's earthquake geology, *Tectonophysics*, *453*, 20–43, doi:10.1016/j.tecto.2007.04.014.

Bayart, E., A. Rubin, and C. Marone (2006), Evolution of fault friction following large velocity jumps, Abstract S31A-0180 presented at 2006 Fall Meeting, AGU, San Francisco, Calif., 5–9 Dec.

Beeler, N. M., T. E. Tullis, and J. D. Weeks (1994), The role of time and displacement in the evolution effect in rock friction, *Geophys. Res. Lett.*, *21*, 1987–1990, doi:10.1029/94GL01599.

Ben-Zion, Y. (2001), Dynamic ruptures in recent models of earthquake faults, *J. Mech. Phys. Solids*, *49*, 2209–2244, doi:10.1016/S0022-5096(01)00036-9.

Ben-Zion, Y., and C. G. Sammis (2003), Characterization of fault zones, *Pure Appl. Geophys.*, *160*, 677–715, doi:10.1007/PL00012554.

Blanpied, M. L., D. A. Locker, and J. D. Byerlee (1991), Fault stability inferred from granite sliding experiments at hydrothermal conditions, *Geophys. Res. Lett.*, *18*, 609–612, doi:10.1029/91GL00469.

Blanpied, M. L., C. J. Marone, D. A. Lockner, J. D. Byerlee, and D. P. King (1998), Quantitative measure of the variation in fault rheology due to fluid-rock interactions, *J. Geophys. Res.*, *103*, 9691–9712, doi:10.1029/98JB00162.

Boatwright, J., and M. Cocco (1996), Frictional constraints on crustal faulting, *J. Geophys. Res.*, *101*, 13,895–13,909, doi:10.1029/96JB00405.

Bos, B., and C. J. Spiers (2000), Effect of phyllosilicates on fluid-assisted healing of gouge-bearing faults, *Earth Planet. Sci. Lett.*, *184*, 199–210, doi:10.1016/S0012-821X(00)00304-6.

Bos, B., and C. J. Spiers (2002), Fluid-assisted processes in gouge-bearing faults: Insights from experiments on a rock analogue system, *Pure Appl. Geophys.*, *159*, 2537–2566, doi:10.1007/s00024-002-8747-2.

Brace, W. F., and J. D. Byerlee (1966), Stick-slip as a mechanism for earthquakes, *Science*, *153*, 990–992, doi:10.1126/science.153.3739.990.

Bullock, R. J., N. De Paola, R. E. Holdsworth, and J. Trabucho-Alexandre (2014), Lithological controls on the deformation mechanisms operating within carbonate-hosted faults during the seismic cycle, *J. Struct Geol.*, *58*, 22–42, doi:10.1016/j.jsg.2013.10.008.

Carpenter, B. M., M. J. Ikari, and C. Marone (2011), Mineralogical controls of fault healing in natural and simulated gouges with implications for fault zone processes and the seismic cycle, Abstract T33E-2457 presented at 2011 Fall Meeting, AGU, San Francisco, Calif., 5-9 Dec.

Cheloni, D., et al. (2014), Coseismic and post-seismic slip of the 2009 L'Aquila (central Italy) MW 6.3 earthquake and implications for seismic potential along the Campotosto fault from joint inversion of high-precision levelling, InSAR and GPS data, *Tectonophysics*, *622*, 168–185, doi:10.1016/j.tecto.2014.03.009.

Chiarabba, C., L. Jovane, and R. DiStefano (2005), A new view of Italian seismicity using 20 years of instrumental recordings, *Tectonophysics*, *295*, 251–268, doi:10.1016/j.tecto.2004.09.013.
Chiaraluce, L. (2012), Unravelling the complexity of Apenninic extensional fault systems: A review of the 2009 L'Aquila earthquake (Central Apennines, Italy), *J. Struct. Geol.*, *42*, 2–18, doi:10.1016/j.jsg.2012.06.007.
Chiaraluce, L., W. L. Ellsworth, C. Chiarabba, and M. Cocco (2003), Imaging the complexity of an active normal fault system: The 1997 Colfiorito (central Italy) case study, *J. Geophys. Res.*, *108*(B6), 2294, doi:10.1029/2002JB002166.
Cirella, A., A. Piatanesi, E. Tinti, M. Chini, and M. Cocco (2012), Complexity of the rupture process during the 2009 L'Aquila, Italy earthquake, *Geophys. J. Int.*, *190*, 607–621, doi:10.1111/j.1365-246X.2012.05505.x.
Collettini, C., M. R. Barchi, L. Chiaraluce, F. Mirabella, and S. Pucci (2003), The Gubbio fault: Can different methods give pictures of the same object?, *J. Geodyn.*, *36*, 51–66, doi:10.1016/S0264-3707(03)00038-3.
Collettini, C., C. Viti, S. A. F. Smith, and R. E. Holdsworth (2009), Development of interconnected talc networks and weakening of continental low-angle normal faults, *Geology*, *37*, 567–570, doi:10.1130/G25645A.1.
Collettini, C., A. R. Niemeijer, C. Viti, S. A. F. Smith, and C. Marone (2011), Fault structure, frictional properties and mixed-mode fault slip behaviour, *Earth Planet. Sci. Lett.*, *311*, 316–327, doi:10.1016/j.epsl.2011.09.020.
Collettini, C., B. M. Carpenter, S. Mollo, and C. Viti (2013), The role of decarbonation in seismicity: A study of the mechanical behaviour of portlandite, Abstract S33D-2445 presented at 2013 Fall Meeting, AGU, San Francisco, Calif., 9-13 Dec.
Collettini, C., B. M. Carpenter, C. Viti, F. Cruciani, S. Mollo, T. Tesei, F. Trippetta, L. Valoroso, and L. Chairaluce (2014), Fault structure and slip localization in carbonate-bearing normal faults: An example from the Northern Apennines of Italy, *J. Struct. Geol.*, *67*, 154–166, doi:10.1016/j.jsg.2014.07.017.
D'Agostino, N., D. Cheloni, G. Fornaro, R. Giuliani, and D. Reale (2012), Space-time distribution of afterslip following the 2009 L'Aquila earthquake, *J. Geophys. Res.*, *117*, B02402, doi:10.1029/2011JB008523.
De Paola, N., T. Hirose, T. Mitchell, G. Di Toro, C. Viti, and T. Shimamoto (2011), Fault lubrication and earthquake propagation in thermally unstable rocks, *Geology*, *39*, 35–38, doi:10.1130/G31398.1.
Den Hartog, S. A. M., and C. J. Spiers (2013), Influence of subduction zone conditions and gouge composition on frictional slip stability of megathrust faults, *Tectonophysics*, *600*, 75–90, doi:10.1016/j.tecto.2012.11.006.
Di Stefano, R., C. Chiarabba, L. Chiaraluce, M. Cocco, P. De Gori, D. Piccinini, and L. Valoroso (2011), Fault zone properties affecting the rupture evolution of the 2009 (MW 6.1) L'Aquila earthquake (central Italy): Insights from seismic tomography, *Geophys. Res. Lett.*, *38*, L10310, doi:10.1029/2011GL047365.
Dieterich, J. H. (1978), Time-dependent friction and the mechanics of stick-slip, *Pure Appl. Geophys.*, *116*, 790–805.
Dieterich, J. H. (1979), Modeling of rock friction: 1. Experimental results and constitutive equations, *J. Geophys. Res.*, *84*, 2161–2168, doi:10.1029/JB084iB05p02161.
Dieterich, J. H., and B. D. Kilgore (1994), Direct observation of frictional contacts: New insights for state-dependent properties, *Pure Appl. Geophys.*, *143*, 283–302, doi:10.1007/BF00874332.
Faulkner, D. R., C. A. L. Jackson, R. J. Lunn, R. W. Schlische, Z. K. Shipton, C. A. J. Wibberley, and M. O. Withjack (2010), A review of recent developments concerning the structure, mechanics and fluid flow properties of fault zones, *J. Struct. Geol.*, *32*, 1557–1575, doi:10.1016/j.jsg.2010.06.009.566.
Fondriest, M., S. A. F. Smith, T. Candela, S. B. Nielsen, K. Mair, and G. Di Toro (2013), Mirror like faults and power dissipation during earthquakes, *Geology*, *41*, 1175–1178, doi:10.1130/G34641.1.
Gratier, J. P., D. K. Dysthe, and F. Renard (2013), The role of pressure solution creep in the ductility of the Earth's upper crust, *Adv. Geophys.*, *54*, 47–179, doi:10.1016/B978-0-12-380940-7.00002-0.
Gratier, J.-P., F. Renard, and B. Vial (2014), Postseismic pressure solution creep: Evidence and time-dependent change from dynamic indenting experiments, *J. Geophys. Res. Solid Earth*, *119*, 2764–2779, doi:10.1002/2013JB010768.
Haines, S. H., B. Kaproth, C. Marone, D. Saffer, and B. A. van der Pluijm (2013), Shear zones in clay-rich fault gouge: A laboratory study of fabric development and evolution, *J. Struct. Geol.*, *51*, 206–225, doi:10.1016/j.jsg.2013.01.002.
Ikari, M. J., D. M. Saffer, and C. Marone (2007), Effect of hydration state on the frictional properties of montmorillonite-based fault gouge, *J. Geophys. Res.*, *112*, B06423, doi:10.1029/2006JB004748.
Ikari, M. J., A. R. Niemeijer, C. J. Spiers, A. J. Kopf, and D. M. Saffer (2013), Experimental evidence linking slip instability with seafloor lithology and topography at the Costa Rica convergent margin, *Geology*, *41*, 891–844, doi:10.1130/G33956.1.
Kaneko, Y., Y. Fialko, D. T. Sandwell, X. Tong, and M. Furuya (2013), Interseismic deformation and creep along the central section of the North Anatolian Fault (Turkey): InSAR observations and implications for rate-and-state friction properties, *J. Geophys. Res. Solid Earth*, *118*, 316–331, doi:10.1029/2012JB009661.
Karner, S. L., C. Marone, and B. Evans (1997), Laboratory study of fault healing and lithification in simulated fault gouge under hydrothermal conditions, *Tectonophysics*, *277*, 41–55, doi:10.1016/S0040-1951(97)00077-2.
Marone, C. (1998), Laboratory-derived friction laws and their application to seismic faulting, *Annu. Rev. Earth Planet. Sci.*, *26*, 643–696, doi:10.1146/annurev.earth.26.1.643.
Marone, C., and B. Kilgore (1993), Scaling of the critical slip distance for seismic faulting with shear strain in fault zones, *Nature*, *362*, 618–621, doi:10.1038/362618a0.
Marone, C., and D. Saffer (2014), The mechanics of frictional healing and slip instability during the seismic cycle, in *Treatise on Geophysics*, 2nd ed., Elsevier, Oxford, U. K., doi:10.1016/B978-0-444-53802-4.00092-0, in press.
Marone, C., and C. H. Scholz (1988), The depth of seismic faulting and the upper transition from stable to unstable slip regimes, *Geophys. Res. Lett.*, *15*, 621–624, doi:10.1029/GL015i006p00621.
Marone, C., C. H. Scholz, and R. Bilham (1991), On the mechanics of earthquake afterslip, *J. Geophys. Res.*, *96*, 8441–8452, doi:10.1029/91JB00275.
Marone, C., J. E. Vidale, and W. L. Ellsworth (1995), Fault healing inferred from time dependent variations in source properties of repeating earthquakes, *Geophys. Res. Lett.*, *22*, 3095–3098, doi:10.1029/95GL03076.
Miller, S. A., C. Collettini, L. Chiaraluce, M. Cocco, M. R. Barchi, and B. Kaus (2004), Aftershocks driven by a high pressure CO_2 source at depth, *Nature*, *427*, 724–727, doi:10.1038/nature02251.
Mirabella, F., M. Barchi, A. Lupattelli, E. Stucchi, and M. G. Ciaccio (2008), Insights on the seismogenic layer thickness from the upper crust structure of the Umbria-Marche Apennines (Central Italy), *Tectonics*, *27*, TC1010, doi:10.1029/2007TC002134.
Miyazaki, S., P. Segall, J. Fukuda, and T. Kato (2004), Space time distribution of afterslip following the 2003 Tokachi-oki earthquake: Implications for variations in fault zone frictional properties, *Geophys. Res. Lett.*, *31*, L06623, doi:10.1029/2003GL019410.
Muhuri, S. K., T. A. Dewers, T. E. Scott Jr., and Z. Reches (2003), Interseismic fault strengthening and earthquake-slip instability: Friction or cohesion?, *Geology*, *31*, 881–884, doi:10.1130/G19601.1.

Nakatani, M., and C. H. Scholz (2004), Frictional healing of quartz gouge under hydrothermal conditions: 1. Experimental evidence for solution transfer healing mechanism, *J. Geophys. Res.*, *109*, B07201, doi:10.1029/2001JB001522.
Niemeijer, A. R., and R. L. M. Vissers (2014), Earthquake rupture propagation inferred from the spatial distribution of fault rock frictional properties, *Earth Planet. Sci. Lett.*, *396*, 154–164, doi:10.1016/j.epsl.2014.04.010.
Niemeijer, A., C. Marone, and D. Elsworth (2008), Healing of simulated fault gouges aided by pressure solution: Results from rock analogue experiments, *J. Geophys. Res.*, *113*, B04204, doi:10.1029/2007JB005376.
Noda, H., and N. Lapusta (2013), Stable creeping fault segments can become destructive as a result of dynamic weakening, *Nature*, *493*, 518–521, doi:10.1038/nature11703.
Olsen, M. P., C. H. Scholz, and A. Leger (1998), Healing and sealing of simulated fault gouge under hydrothermal conditions: Implications for fault healing, *J. Geophys. Res.*, *103*(B4), 7421–7430, doi:10.1029/97JB03402.
Parsons, T. (2005), A hypothesis for delayed dynamic earthquake triggering, *Geophys. Res. Lett.*, *32*, L04302, doi:10.1029/2004GL021811.
Peng, Z., J. E. Vidale, C. Marone, and A. Rubin (2005), Systematic variations in recurrence interval and moment of repeating aftershocks, *Geophys. Res. Lett.*, *32*, L15301, doi:10.1029/2005GL022626.
Renard, F., S. Beaupretre, C. Voisin, D. Zigone, T. Candela, D. K. Dysthe, and J.-P. Gratier (2012), Strength evolution of a reactive frictional interface is controlled by the dynamics of contacts and chemical effects, *Earth Planet. Sci. Lett.*, *341*, 20–34, doi:10.1016/j.epsl.2012.04.048.
Rice, J. R. (1993), Spatio-temporal complexity of slip on a fault, *J. Geophys. Res.*, *98*, 9885–9907, doi:10.1029/93JB00191.
Ruina, A. (1983), Slip instability and state variable friction laws, *J. Geophys. Res.*, *88*, 10,359–10,370, doi:10.1029/JB088iB12p10359.
Scholz, C. H. (2002), *The Mechanics of Earthquakes and Faulting*, 2nd ed., Cambridge Press, New York.
Scuderi, M. M., A. R. Niemeijer, C. Collettini, and C. Marone (2013), Frictional properties and slip stability of active faults within carbonate–evaporite sequences: The role of dolomite and anhydrite, *Earth Planet. Sci. Lett.*, *369*, 220–232, doi:10.1016/j.epsl.2013.03.24.
Sjoberg, E. L., and D. T. Rickard (1984), Temperature dependence of calcite dissolution kinetics between 1 and 62°C at pH 2.7 to 8.4 in aqueous solutions, *Geochim. Cosmochim. Acta*, *48*, 485–493.
Smith, S. A. F., A. Billi, G. Di Toro, and R. Spiess (2011), Principal slip zones in limestone: Microstructural characterization and implications for the seismic cycle (Tre Monti Fault, Central Apennines, Italy), *Pure Appl. Geophys.*, *168*, 2365–2393, doi:10.1007/s00024-011-0267-5.
Stewart, I. S., and P. L. Hancock (1991), Scales of structural heterogeneity within neotectonic normal fault zones in the Aegean region, *J. Struct. Geol.*, *13*, 191–204, doi:10.1016/0191-8141(91)90066-R.
Tenthorey, E., S. F. Cox, and H. F. Todd (2003), Evolution of strength recovery and permeability during fluid-rock reaction in experimental fault zones, *Earth Planet. Sci. Lett.*, *206*, 161–172, doi:10.1016/S0012-821X(02)01082-8.
Tesei, T., C. Collettini, M. R. Barchi, B. M. Carpenter, and G. Di Stefano (2014), Heterogeneous strength and fault zone complexity of carbonate-bearing thrusts with possible implications for seismicity, *Earth Planet. Sci. Lett.*, *408*, 307–318, doi:10.1016/j.epsl.2014.10.021.
Trippetta, F., S. Mollo, B. M. Carpenter, and C. Collettini (2013), The relationship between fault Zone processes and physical-transport properties: The carbonate-bearing Monte Maggio Fault (Central Italy), Abstract T53C-2591 presented at 2013 Fall Meeting, AGU, San Francisco, Calif., 9-13 Dec.
Valoroso, L., L. Chiaraluce, D. Piccinini, R. Di Stefano, D. Schaff, and F. Waldhauser (2013), Radiography of a normal fault system by 64,000 high-precision earthquake locations: The 2009 L'Aquila (central Italy) case study, *J. Geophys. Res. Solid Earth*, *118*, 1156–1176, doi:10.1002/jgrb.50130.
Valoroso, L., L. Chiaraluce, and C. Collettini (2014), Earthquakes and fault zone structure, *Geology*, doi:10.1130/G35071.1.
Verberne, B. A., C. He, and C. J. Spiers (2010), Frictional properties of sedimentary rocks and natural fault gouge from the Longmen Shan Fault Zone, Sichuan, China, *Bull. Seismol. Soc. Am.*, *100*, 2767–2790, doi:10.1785/0120090287.
Verberne, B. A., C. J. Spiers, A. R. Niemeijer, J. H. De Bresser, D. A. M. De Winter, and O. Plumper (2013), Frictional properties and microstructure of calcite-rich fault gouges sheared at sub-seismic sliding velocities, *Pure Appl. Geophys.*, doi:10.1007/s00024-013-0760-0.
Violay, M., S. Nielsen, E. Spagnuolo, D. Cinti, G. Di Toro, and G. Di Stefano (2013), Pore fluid in experimental calcite-bearing faults: Abrupt weakening and geochemical signature of co-seismic processes, *Earth Planet. Sci. Lett.*, *361*, 74–84, doi:10.1016/J.Epsl.2012.11.021.
Viti, C., C. Collettini, and T. Tesei (2014), Pressure solution seams in carbonatic fault rocks: Mineralogy, micro/nanostructures and role in deformation mechanism, *Contrib. Mineral. Petrol.*, doi:10.1007/s00410-014-0970-1.
Weeks, J. D., and T. E. Tullis (1985), Frictional sliding of dolomite: A variation in constitutive behavior, *J. Geophys. Res.*, *90*, 7821–7826, doi:10.1029/JB090iB09p07821.
Yasuhara, H., C. Marone, and D. Elsworth (2005), Fault zone restrengthening and frictional healing: The role of pressure solution, *J. Geophys. Res.*, *110*, B06310, doi:10.1029/2004JB00327.
Zhang, X., and C. J. Spiers (2005), Compaction of granular calcite by pressure solution at room temperature and effects of pore fluid chemistry, *Int. J. Rock Mech. Min. Sci.*, *42*, 950–960, doi:10.1016/j.ijrmms.2005.05.017.